

Rapid self-magnetization of laser speckles in plasmas by nonlinear anisotropic instability

A G R Thomas¹, R J Kingham and C P Ridgers

Plasma Physics Group, Imperial College, Blackett Laboratory,
London SW7 2BZ, UK

E-mail: agrt@umich.edu

New Journal of Physics **11** (2009) 033001 (11pp)

Received 12 September 2008

Published 3 March 2009

Online at <http://www.njp.org/>

doi:10.1088/1367-2630/11/3/033001

Abstract. Presented here are the first kinetic two-dimensional Vlasov–Fokker–Planck calculations of inertial confinement fusion-related laser–plasma interactions, to include self-consistent magnetic fields, hydrodynamic plasma expansion and anisotropic electron pressure. An underdense plasma, reminiscent of the gas fill of a hohlraum, is heated by a laser speckle with $I\lambda^2 = 1.0 \times 10^{15} \text{ W cm}^{-2} \mu\text{m}^2$ and radius $w_0 = 5 \mu\text{m}$. Inverse bremsstrahlung absorption of the laser and non-local electron transport lead to the development of a collisional analogue of the Weibel electromagnetic instability. The instability is seeded by magnetic fields, generated in an initial period of linear growth due to the anisotropic electron distribution arising in a laser speckle. Using the circular polarization does not generate significant fields. For linear polarization, the field generally saturates when the magnetization is $\omega\tau_{ei} > 1$, and the effective growth rate is similar to the coherence time of typical laser speckles. The presence of these magnetic fluctuations significantly affects the heat fluxes and hydrodynamics in the plasma.

Contents

1. Introduction	2
2. The model and set-up	3
3. Magnetic field generation by laser speckles	5
4. Conclusions	9
Acknowledgments	10
References	10

¹ Present address: The University of Michigan, Ann Arbor, MI, USA.

1. Introduction

Magnetic field generation in nanosecond timescale, laser generated, collisional plasmas occurs due to a number of mechanisms, each described by a term in Ohm's law. Therefore, the choice of the form of Ohm's law used is crucial in determining the magnetic fields in long pulse laser-plasma interactions. For example, the $\nabla T \times \nabla \ln n$, or thermoelectric, mechanism is a well-known hydrodynamic source of magnetic fields [1, 2]. This occurs due to electric fields that arise to balance scalar electron pressure gradients and maintain quasineutrality in collisional plasmas. Other sources of magnetic fields include divergent non-local fluxes [3], photon momentum deposition [4] and a number of electromagnetic instabilities [5, 6] including Weibel's instability [7]. In general, electron pressure is not isotropic; magnetic fields can also be generated by anisotropic electron pressure, which can be driven by the electron oscillation in the laser field [8]–[12], for example. This generation mechanism is a collisional version of Weibel's collisionless instability [13].

Proper consideration of these magnetic fields is very important, as they are well known to alter the transport properties of the plasma [14]. In experiments, magnetic fields have been observed to affect the long-term evolution of an expanding plasma [15], to suppress non-locality [16], and to be generated and reconnect in laboratory astrophysical experiments [17]. Understanding the role magnetic fields take in suppressing heat flow is particularly important in laser fusion scenarios, such as hohlraums [18]. Such magnetic fields are significant, in that their presence affects the magnitude and direction of the particle fluxes, e.g. electron heat flux, and therefore the long-time evolution of the system. This evidently has consequences for inertial fusion energy applications, as the coupling of the laser beams with the walls or pellet and the development of hot spots are all critical to the uniformity of the implosion; the inhibition of transport due to magnetic fields can lead to these hot spots which can in turn inhibit the onset of back-scattering instabilities [19].

The lasers used for inertial confinement fusion (ICF) will have their intensity profiles randomly distributed in a series of hot spots, or speckles of high intensity, by the use of random phase plates [20]. The speckle pattern has a coherence time of less than the hydrodynamic timescale (1–10 ps), so that the ion fluid experiences a relatively uniform, time averaged, heating profile [21]. However, since the source of magnetic field generation is proportional to the gradients in electron pressure and laser intensity, these small scale-length speckles can be significant sources of magnetic field, and therefore the resulting fields can affect the hydrodynamics over longer timescales. Under such conditions of small temperature scale lengths due to speckles, non-local effects can also play a significant role in affecting the transport properties of the plasma [22]. Hence, accurate modelling of both magnetic fields and non-local effects are important in determining the evolution of a system.

In this paper, magnetic field generation by circular laser speckles was analysed by the first kinetic, two-dimensional, Vlasov–Fokker–Planck (VFP) code designed for ICF-related scenarios to include self-consistent magnetic fields, hydrodynamic plasma expansion and anisotropic electron pressure. The parameters used were similar to those used by Dubroca *et al* [11], allowing comparison with the ten moment fluid calculations used in that investigation. Here, the more detailed VFP treatment, over a 50 ps timescale, resulted in magnetization of the plasma for linear polarization of over an order of magnitude greater than with the hydrodynamic calculation. Additionally, the growth rate of the fields was significantly less than 10 ps, which is within the typical coherence time of a laser speckle, when the Cartesian tensor distribution

function expansion [23] included terms up to order 2. When a reduced model for the full rank 3 heat-flux tensor was included, the growth rate was damped but remained significant in terms of the long-time evolution of the system. The simplicity of the equation used for the heat flux tensor would also mean it would tend to overestimate the damping.

The reason for the rapid growth of strong magnetic fields is that the calculations in this study self-consistently included the feedback of the magnetic field on the electrons, in addition to non-local electron transport arising naturally from the VFP calculation. The result of the feedback is that a collisional analogue of the Weibel instability driven by the laser field occurs [8]–[10], which amplifies a seed field generated by the spatial variation in anisotropic pressure [11]. Although a linear, local analysis of the Weibel instability driven by inverse bremsstrahlung (IB) heating suggests the growth rates are too small to be a problem for ICF scenarios [24], in the nonlinear and non-local regime studied here, the effective growth rate is sufficient to magnetize the plasma within the lifetime of a speckle. Consequently, heat flux and ion flux across a large number of similar magnetic perturbations are expected to be modulated, leading to a modification of the transport properties.

2. The model and set-up

The VFP equation provides a fully kinetic description of semi-collisional plasmas. It describes the evolution of a particle distribution function in the presence of macroscopic electromagnetic fields and microscopic small-angle deflections:

$$\left[\frac{\partial}{\partial t} + \underline{v} \cdot \nabla - \frac{e}{m_e} (\underline{E} + \underline{v} \times \underline{B}) \cdot \frac{\partial}{\partial \underline{v}} \right] f(\underline{v}, \underline{r}, t) = - \frac{\partial}{\partial \underline{v}} \cdot \{ f(\underline{v}, \underline{r}, t) \langle \Delta \underline{v} \rangle \} + \frac{1}{2} \frac{\partial}{\partial \underline{v}} \frac{\partial}{\partial \underline{v}} : \{ f(\underline{v}, \underline{r}, t) \langle \Delta \underline{v} \Delta \underline{v} \rangle \}. \quad (1)$$

Here, \underline{E} and \underline{B} are the macroscopic electric and magnetic fields and $f \, d^3 \underline{r} \, d^3 \underline{v}$ represents the number of particles within a phase-space volume of $d^3 \underline{r} \, d^3 \underline{v}$. The terms on the right-hand side represent drag and diffusion in velocity space, respectively, and sum to zero for a maxwellian particle velocity distribution. Ampère–Maxwells' and Faraday's laws provide the necessary equations to calculate the evolution of fields and distribution function, given some initial conditions:

$$\nabla \times \underline{B} = \mu_0 \underline{j} + \frac{1}{c^2} \frac{\partial \underline{E}}{\partial t}, \quad (2)$$

$$\nabla \times \underline{E} = - \frac{\partial \underline{B}}{\partial t}. \quad (3)$$

Since the distribution function is six dimensional, solving using this formalism can be computationally difficult. Various methods can be used to reduce the problem. Here a Cartesian tensor expansion [23] is employed, with the distribution function expanded as $f(t, \underline{r}, \underline{v}) = f_0 + \underline{f}_1 \cdot \underline{\hat{v}} + \underline{\underline{f}}_2 : \underline{\hat{v}} \underline{\hat{v}} + \dots$. This expansion can be truncated in a collisional plasma, as collisions tend to push the distribution towards an isotropic distribution, in the centre of mass frame, represented by f_0 . Higher orders are successively smaller perturbations, $f_0 \gg f_1 \gg f_2 \dots$, but this ordering does not necessarily hold for all \underline{v} , i.e. in the tail of the distribution. Physically measurable quantities relate to the terms in the expansion via moments; integrals over the

velocity space. When considering the electron distribution, f_0 yields scalar quantities such as electron density n_e and temperature T_e . f_1 yields vector quantities such as current j and scalar total electron heat flux q_e . f_2 is related to the anisotropic pressure tensor $\underline{\underline{P}}_e$, in a marginally more complicated way;

$$m_e \frac{8\pi}{15} \int_0^\infty \underline{\underline{f}}_2 v^4 dv = \underline{\underline{P}}_e - \frac{1}{3} I p_e = \underline{\underline{\Pi}}_e, \quad (4)$$

where p_e is the scalar electron pressure.

A planar, CH plasma with an initially uniform, unmagnetized density profile and uniform temperature was modelled using a second generation of the VFP code IMPACT [25]. The new code, IMPACTA, uses the same basic model as IMPACT, but includes a number of improvements, most notably the addition of the second-order term in the Cartesian tensor expansion of the distribution function, which allows Weibel-like instabilities to occur. In this model, the VFP equation is solved for the electron distribution, but the ions are treated as a cold fluid.

The plasma was subsequently heated by a collimated, non-evolving, circular laser beam, which was modelled in an x - y -plane perpendicular to its propagation. Laser heating was implemented using an operator that is a modification of Langdon's [26] for IB laser heating. This includes the effects of the laser field on the anisotropy of the distribution and also the feedback of magnetic fields on the absorption process. The new part of the heating operator is obtained by following the same method as Langdon, but by both substituting the time averaged f_1 generated by the laser field into the f_2 equation and including a quasi-static background magnetic field. The oscillation of electrons in the laser field tends to distort the distribution function, giving it an ellipticity in velocity space. The presence of the magnetic field does not affect f_0 , but rotates the absorption of anisotropic pressure from the component in the direction of polarization into the other components. The IB operator for f_2 that includes these effects is

$$\left. \frac{\partial \underline{\underline{f}}_2}{\partial t} \right|_{\text{IB}} = \frac{1}{2} Y n_i Z^2 v_0^2 \left[\left(\underline{\underline{P}}_{\text{IB}} + \underline{\underline{P}}_{\text{B}} \right) v \frac{\partial}{\partial v} \left(\frac{1}{v^4} \frac{\partial}{\partial v} f_0 \right) + \frac{3}{v^4} \underline{\underline{P}}_{\text{B}} \frac{\partial}{\partial v} f_0 \right], \quad (5)$$

where $\underline{\underline{P}}_{\text{IB}} = (\widehat{\underline{\underline{E}}}_{\text{L}} \widehat{\underline{\underline{E}}}_{\text{L}} - \frac{1}{3} \mathbb{I})$ is a tensor describing the effect of the polarization direction ($\widehat{\underline{\underline{E}}}_{\text{L}}$) of the laser, and $\underline{\underline{P}}_{\text{B}} = (1/2\nu_{\text{ei}})(\widehat{\underline{\underline{E}}}_{\text{L}} \underline{\underline{\omega}}_{\text{c}} \times \widehat{\underline{\underline{E}}}_{\text{L}} + \underline{\underline{\omega}}_{\text{c}} \times \widehat{\underline{\underline{E}}}_{\text{L}} \widehat{\underline{\underline{E}}}_{\text{L}})$ describes the feedback of the magnetic field on the absorption of laser momentum. $Y = 4\pi(e^2/4\pi\epsilon_0 m_e)^2 \ln \Lambda_{\text{ei}}$, and $\ln \Lambda_{\text{ei}}$ is the Coulomb logarithm for electron-ion (e-i) scattering. Also, $1/\nu_{\text{ei}} \propto v^3$ is the mean 90° scattering time for an electron of speed v from the ion background, and $\omega_{\text{c}} = eB/m_e$ is the electron cyclotron frequency. It has been assumed that the feedback of this anisotropic pressure on the laser oscillation current is negligible. This expression is equivalent to those given in [24, 27], but in Cartesian expanded form. In the case of circular polarization, where the electric field direction is changing as a function of time, the cycle average of the dyadic $\widehat{\underline{\underline{E}}}_{\text{L}} \widehat{\underline{\underline{E}}}_{\text{L}}$ is used. Further details of the derivation of the modified heating operator will be given in a future publication.

The new code, IMPACTA, uses an implicit finite difference algorithm to solve the components of the expanded VFP equation for electrons, in addition to the Faraday and the Ampère-Maxwell equations for the fields. Note that in IMPACT, the magnetic field was calculated explicitly. IMPACTA currently uses the Lorentz approximation (valid for high Z), whereby electron-electron (e-e) collisions are neglected in the equation for f_1 and higher. The change in f_l due to e-i scattering is retained in all equations, in the reduced form, where it

is $\delta f_i / \delta t \propto -f_i l(l+1)/2v^3$. All terms in $\partial/\partial t$ are retained. A hydrodynamic ion fluid model is included using the equations used in [28], but with the full electron pressure tensor used to update the ion velocity.

The ambient electron number density, mean ionization state, mean atomic mass and initial temperature of the plasma were taken to be $n_{e0} = 1 \times 10^{20} \text{ cm}^{-3}$, $\bar{Z} = 5$, $\bar{A} = 6.5$ and $T_{e0} = 1 \text{ keV}$, respectively. These conditions would be relevant to the gas fill of a hohlraum used for indirect drive ICF. Under these conditions, the mean-free path and collision time, for angular scattering of an electron (moving at the initial thermal speed $v_{t0} = \sqrt{2k_b T_{e0}/m_e}$) by the ion background, were $\lambda_{ei} = 4.0 \mu\text{m}$ and $\tau_{ei} = 214 \text{ fs}$, respectively, and the Coulomb logarithm was $\ln \Lambda_{ei} = 7.6$. The size of the computational domain was a square of side $192 \mu\text{m}$. The spatial domain used a square grid with a constant spacing of $\Delta x, \Delta y = 0.625 \mu\text{m}$ in the vicinity of the heated region (a central $50 \mu\text{m} \times 50 \mu\text{m}$ square). Grid cells near to the boundary exponentially increased in size to a boundary cell size of $42 \mu\text{m}$, to ensure heat flowed away from the vicinity of the speckle, with reflecting boundary conditions. The velocity grid was defined as $0 < v < 12v_{t0}$, with spacing $\Delta v = 0.1v_{t0}$. The laser profile was a circular, Gaussian intensity profile with a radius of $5 \mu\text{m}$ at $1/e$ of full intensity, and with heating strength was $I\lambda^2 = 1.0 \times 10^{15} \text{ W cm}^{-2} \mu\text{m}^2$. These conditions are similar to those studied in [11]. The full duration of the numerical integration was 52 ps , with a time step of $\Delta t = 20 \text{ fs}$.

3. Magnetic field generation by laser speckles

The calculations performed here demonstrated growth rates of up to 0.56 ps^{-1} for magnetic fields generated around a circular speckle, typical of the laser profiles propagating through the gas fill of a hohlraum. Even the most conservative calculation yielded a Hall parameter of $\omega_c \tau_{ei} > 0.1$ within 10 ps . The structure of the magnetic field was initially always a quadrupole around the heating region, as shown in figure 1(a). This structure is due to the linear magnetic field growth associated with the electric field that balances the anisotropic pressure. The independent, nonzero components of the traceless part of the pressure tensor, $\underline{\Pi}_e = \underline{P}_e - (1/3)\underline{I}p_e$, can be expressed in this coordinate system in the combination $\Delta \Pi_e = (\Pi_{xx} - \Pi_{yy})/2$ and Π_{xy} , where \underline{P}_e is the full pressure tensor, and p_e is the scalar pressure [11].

For early times, when the magnetic field is weak, as in figure 1, $\Delta \Pi_e$ is approximately the same shape as the heating profile. This is because collisions with ions transfer the distortion of the distribution function due to the oscillation of electrons in the laser field, and therefore increases Π_{xx} , for linear polarization in x , and decreases Π_{yy} . The deviation from a circular region for $\Delta \Pi_e$ is due to transport; the pressure tensor is also affected by gradients in temperature. The contribution to the electric field from the pressure tensor can be found by taking moments of the expanded VFP equation, but for a Maxwellian velocity distribution is proportional to $\nabla \cdot \underline{P}_e / n_e$. This term is a more general form of the thermoelectric magnetic field generation mechanism, where the electric field is proportional to $\nabla p_e / n_e$. On taking the curl of the electric field to find the magnetic field source, in this planar Cartesian geometry, two terms arise;

$$\frac{\partial B}{\partial t} \propto \frac{\partial}{\partial x} \frac{\partial}{\partial y} \Delta \Pi_e + \left(\frac{\partial^2}{\partial x^2} - \frac{\partial^2}{\partial y^2} \right) \Pi_{xy}. \quad (6)$$

The first of these leads to the quadrupole magnetic field structure shown in figure 1(a).

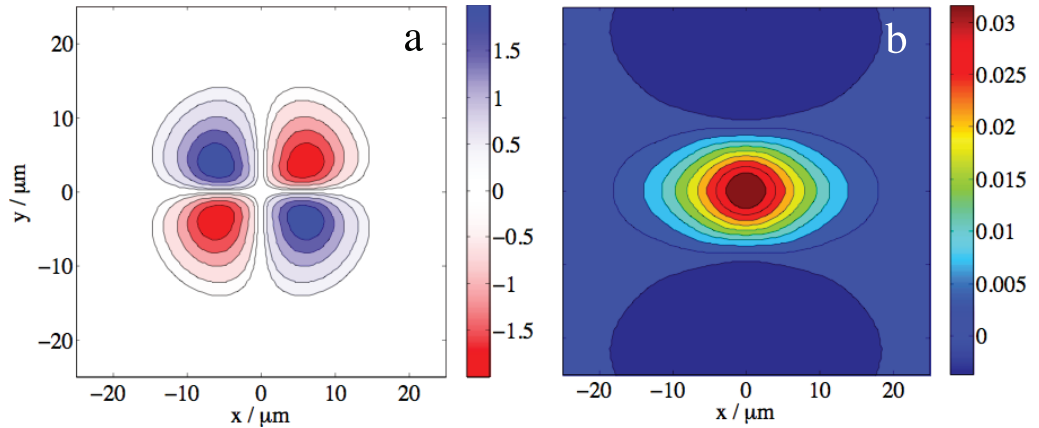


Figure 1. (a) Magnetic field, B_z , in tesla and (b) $\Delta\Pi_e$ normalized to $n_{e0}kT_{e0}$ after laser heating by a $5\ \mu\text{m}$ speckle for $t = 2\ \text{ps}$. The laser is linearly polarized in the x -(horizontal) direction.

Later in time, the structure changes to a more complicated magnetic field shape, arising due to the onset of the feedback of the magnetic field on $\underline{\Pi}_e$ itself and involves the second term of equation (6). The magnetic field rotates the distribution slightly, leading to a two-dimensional version of the collisional Weibel instability occurring. In figure 2, the magnetic fields, $\Delta\Pi_e$ and Π_{xy} , are shown after 4 ps, in the same calculation as before. The magnetic field structure is still a quadrupole, but is now much stronger closer to the x -axis. The effect of the magnetic field can clearly be seen in the diagonal components of the traceless pressure tensor, $\Delta\Pi_e$, where it has been eroded away in the presence of the magnetic field. As can be seen from figure 2, $\Delta\Pi_e$ has been rotated into Π_{xy} . The magnetic field generation that results is now the combination of both sources in equation (6).

In this calculation, the growth rate of the magnetic field was such that it exceeded a Hall parameter of $\omega_c\tau_{ei} > 1$ in 6 ps. After that initial fast growth, the Nyquist wavelength components of the field on the grid started to dominate, as these grow faster than the wavelengths that are resolved. The growth rate of the collisional Weibel instability with the expansion to f_2 , as employed in this particular calculation, is known to be too fast for the largest values of k (small-wavelength perturbations) [29]. This is because the next order (f_3) acts as a diffusive term for the anisotropic pressure. To include the effects of f_3 is currently computationally difficult for this implicit method. However, it can be included in the equation for f_2 in a reduced form. For this, only the spatial and collisional terms in the f_3 equation are considered, which can be rearranged and then substituted into the f_2 equation. The details of this will be given in a future publication. This has the effect of dramatically reducing the growth rate for large k . However, it tends to over-estimate the damping, as the feedback of the magnetic field, and the inhibiting effect of the electric field on f_3 are not included.

When the same calculations were performed with this ‘Weibel damping’ included, the growth rate was dramatically reduced. The grid-limited (largest k) wavenumber magnetic field perturbations were damped away completely, and the growth rate of the resolved instability was lowered by more than an order of magnitude. Even under the conditions of this damping, the growth of magnetic field was fast enough that the plasma was magnetized sufficiently ($\omega_c\tau_{ei} \approx 0.1$), within the coherence time of a typical speckle ($< 10\ \text{ps}$), to suppress and redirect

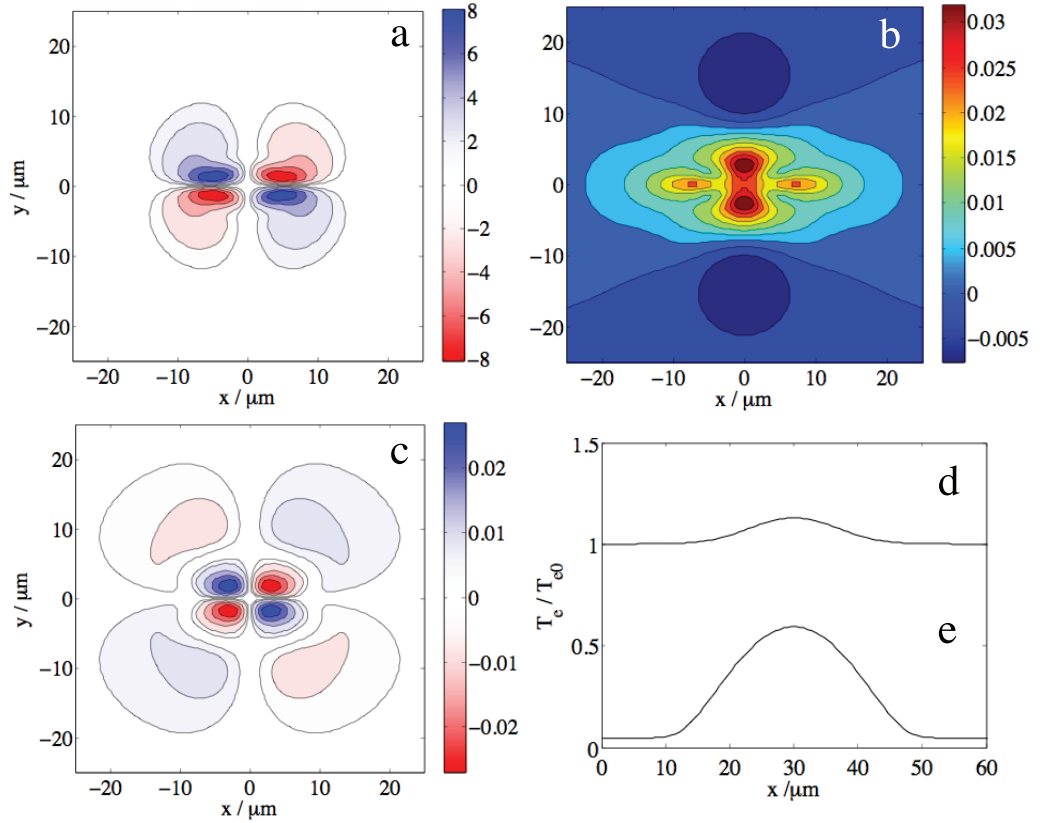


Figure 2. (a) Magnetic field, B_z , in tesla, (b) $\Delta\Pi_e$ normalized to $n_{e0}kT_{e0}$ and (c) Π_{xy} normalized to $n_{e0}kT_{e0}$ after laser heating of a 1 keV plasma by a $5\ \mu\text{m}$ speckle for $t = 4\ \text{ps}$. The laser is linearly polarized in the x (horizontal)-direction. (d, e) The temperature profile of the plasma normalized to T_{e0} after 2.2 ps of heating for calculations with initial temperatures of (d) 1 keV and (e) 20 eV.

heat flow. This would lead to a transport barrier, leading to a higher temperature in the laser heating region than would otherwise exist. This could suppress back-scattering instabilities, and therefore increase the coupling efficiency of the laser. Note that even though the growth rate changed with this addition to the model, the qualitative behaviour remained the same.

The calculations were also performed with the initial ambient temperature being 20 eV instead of 1 keV as before. In this case, non-local effects were strong due to the small scale-length gradients in temperature that occur as the plasma rapidly heats. The heating is sufficiently rapid that the temperature at the centre of the spot is of the same order of magnitude as before (and hence still non-local), but the gradients in temperature are more pronounced, figures 2(d) and (e). This situation would represent early time behaviour in the gas fill of a hohlraum. The magnetic fields that were generated grow rapidly even with ‘Weibel damping’ switched on. A magnetization of $\omega_c \tau_{ei} > 1$ was achieved in 25 ps, which considering that this represents a conservative calculation is significant. In this case the interaction is particularly complicated. The magnetic field source from non-local effects given by Kingham and Bell [3] is zero here, due to the circular symmetry. Here, it is the interaction between the non-local and anisotropic effects which leads to the magnetic field growth.

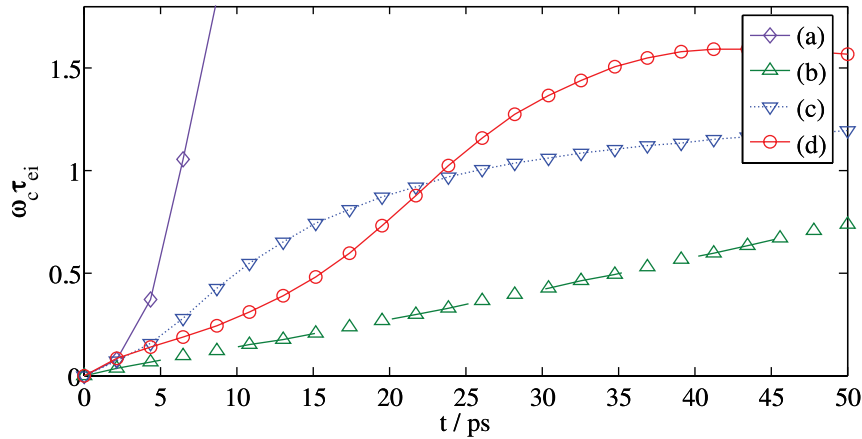


Figure 3. Effective magnetization, $\omega_c \tau_{ei0}$ for calculations under the conditions given in the text for (a) no ‘Weibel damping’, $T_{e0} = 1$ keV, including $\underline{P}_{\underline{B}}$; (b) with ‘Weibel damping’, $T_{e0} = 1$ keV, including $\underline{P}_{\underline{B}}$; (c) no ‘Weibel damping’, $T_{e0} = 1$ keV, $\underline{P}_{\underline{B}} = 0$ and (d) with ‘Weibel damping’, $T_{e0} = 20$ eV, including $\underline{P}_{\underline{B}}$.

In figure 3, time histories of the maximum effective magnetization in these calculations are given. The calculations were all performed with identical laser parameters and under the same initial plasma conditions as described above, except for the following differences: figure 3(a) was run with the expansion of the distribution function up to f_2 and self-consistently contained the feedback of the quasi-static magnetic field on the absorption of anisotropy from the laser ($\underline{P}_{\underline{B}}$ from equation (5)). This gave a very fast growth rate (0.56 ps^{-1}) for the magnetic quadrupole around the speckle. Due to the strong feedback, after 6 ps the wavelength of the field structure rapidly approached the grid Nyquist wavelength. The feedback of the magnetic fields on the absorption acted to increase the spatial gradients in the pressure tensor, and therefore enhance magnetic field generation. Under the same conditions, but including the reduced model for f_3 , figure 3(b), the growth rate is dramatically reduced, and the linear growth dominates. In figure 3(c), the reduced f_3 model was not included, and also $\underline{P}_{\underline{B}} = 0$. In this case, the growth rate is reduced compared with figure 3(a), indicating that the feedback of the magnetic field enhances the generation mechanism. As the calculation does not go numerically unstable, the field can be seen to initially grow rapidly, but then saturate at a magnetization of $\omega_c \tau_{ei0} \approx 1$. Finally, figure 3(d) shows a calculation with the same model as in figure 3(b), but starting with a lower ambient temperature of 20 eV. The effect of the transport induced by the associated temperature gradients was to dramatically increase the growth rate, even for this conservative calculation. The growth of strong magnetic fields was characteristic of all calculations that included the effect of anisotropic pressure and linear polarization. It is worth noting that with circular polarization, under these conditions, no magnetic fields were generated. The reason for this is that, although circular polarization does generate anisotropic pressure, it is azimuthally symmetric in the polarization plane.

The effects of this magnetization on transport is shown in figure 4. The magnitude of heat flux is shown in figure 4(a), for an initially 20 eV calculation after 50 ps of heating. It is modulated substantially by the combined effects of the generated magnetic fields and spatially asymmetric pressure tensor. The effect on transport is evidently most clearly seen for the low

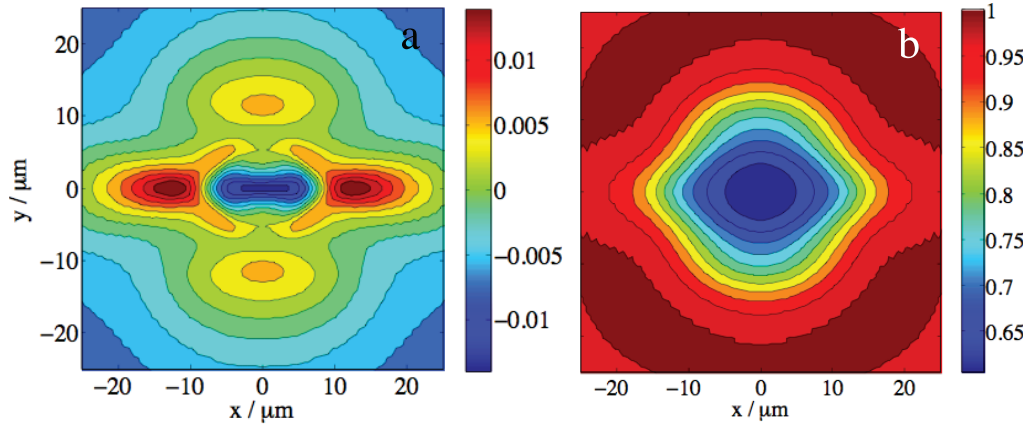


Figure 4. (a) The magnitude of normalized heat flux, $\sqrt{m_e}q/(2k_b T_{e0})^{3/2}n_{e0}$ and (b) the normalized ion number density, n_i/n_{i0} of an initially 20 eV plasma after 50 ps heating.

initial temperature calculations, as the increased temperature gradients lead to more pronounced heat flows and ion velocities. The ion number density after 50 ps, figure 4(b), has a profile that is also very non-symmetric, due to the combined effects of the magnetic fields in suppressing heat flow and anisotropic pressure, and indirectly affecting the ion velocity, \underline{C}_i through the $\underline{B} \times \underline{C}_i$ correction to the electric field. In a large-scale calculation, the effect of these magnetic fluctuations would be to modulate the heat flux and ion velocity, leading to a non-uniform distribution of energy density in the plasma.

4. Conclusions

In the calculations performed in this paper, strong magnetic fields were generated in times that are very short in the context of nanosecond laser interactions. The fields were generated in quadrupole structures around laser speckles occurring in the laser profiles. Although the laser is smoothed over the hydrodynamic timescale, the rapidity of the growth of these fields could, very feasibly, sufficiently magnetize the plasma within the coherence time of a laser speckle. It would therefore be of interest to consider the effect of a plasma containing a quasi-randomly distributed collection of alternating magnetic field regions. A calculation of transport in a plasma with this magnetic field structure should result in modified heat flow and hydrodynamics. This could also be further enhanced, because the magnetic fields are advected with the heat flow, and therefore compress and amplify [6], resulting in a potential barrier to further heat flow. This is left for further work.

As the calculations performed here are for almost identical conditions to [11], it is worth noting the major differences from that study. The main conclusion, that these laser speckles can result in magnetic field generation is broadly the same, despite the former calculation being a hydrodynamic calculation, as opposed to the kinetic result here. However, the effect of the feedback of the magnetic field on the IB absorption of anisotropic pressure, which is included here, results in a magnetic field generating instability. This two-dimensional analogue of the collisional Weibel instability causes the fields to be strongly amplified from the linear mechanism of [11]. Other differences include a quadrupole instead of octopole structure, which

arises from non-local flows suppressing the gradient in the *shape*² of the electron distribution function, and the saturation of the field; in this calculation, saturation occurs due to suppression of the driving $\Delta\Pi_e$ due to the magnetic field. In [11], saturation is due to the Nernst effect [31]. Here, flux limiters are not required and the Nernst effect is included, both naturally because of the VFP calculation. Hence the rate of Nernst advection differs due to the heat flow differing from the hydrodynamic calculation.

Note that under the conditions studied here, the effect of f_2 due to pressure gradients is not normally significant either [32]. However, the laser generated anisotropy and the collisional Weibel instability mean that inclusion of f_2 is important. f_3 represents the flows and diffusion of f_2 , and hence its importance only arises when gradients in f_2 become very large, as for high k Weibel modes. The inclusion of f_3 in a reduced manner does dramatically reduce the magnetic field growth. However, this reduced model is likely to overestimate the damping, due to the neglecting of magnetic and electric fields in the f_3 equation. A full calculation may be possible in the future, but as is, this represents a ‘reality check’ on the results obtained here. *Since significant fields are still generated even with the reduced model*, it is highly probable that laser speckles do generate quasistatic magnetic fields, which redirect and inhibit global heat flow. This magnetic field generation can be eliminated (in this geometry) by the use of circularly polarized radiation.

Acknowledgments

AGRT acknowledges financial supported from AWE plc, Aldermaston. IMPACTA was developed with financial support from EPSRC under grant EP/C531566/1.

References

- [1] Stamper J A and Ripin B H 1975 Faraday-rotation measurements of megagauss magnetic-fields in laser-produced plasmas *Phys. Rev. Lett.* **34** 138–41
- [2] Craxton R S and Haines M G 1975 Hot spots in laser plasmas *Phys. Rev. Lett.* **35** 1336–9
- [3] Kingham R J and Bell A R 2002 Nonlocal magnetic-field generation in plasmas without density gradients *Phys. Rev. Lett.* **88** 045004
- [4] Haines M G 2001 Generation of an axial magnetic field from photon spin *Phys. Rev. Lett.* **87** 135005
- [5] Tidman D A and Shanny R A 1974 Field-generating thermal instability in laser-heated plasmas *Phys. Fluids* **17** 1207–10
- [6] Brownell J H 1979 Magnetic-field generation in implosions due to nernst refrigeration *Comments Plasma Phys. Control. Fusion* **4** 131–8
- [7] Weibel E S 1959 Spontaneously growing transverse waves in a plasma due to an anisotropic velocity distribution *Phys. Rev. Lett.* **2** 83–4
- [8] Romanov A Y, Silin V P and Uryupin S A 1997 Weibel instability associated with inverse bremsstrahlung absorption of intense electromagnetic radiation *J. Exp. Theor. Phys.* **84** 687–93
- [9] Bendib A, Bendib K and Sid A 1997 Weibel instability due to inverse bremsstrahlung absorption *Phys. Rev. E* **55** 7522–6

² IB heating tends to distort the electron distribution function from a super-Gaussian of order 2 (i.e. a Maxwellian) towards a super-Gaussian of order 5. Spatial gradients in the *order* of the underlying super-Gaussian distribution may lead to magnetic field generation, as can be seen by consideration of the modified transport coefficients derived in [30].

- [10] Ferrante G, Zarcone M and Uryupin S A 2001 Plasma electron kinetics in a weak high-frequency field and magnetic field amplification *Phys. Rev. E* **64** 046408
- [11] Dubroca B, Tchong M, Charrier P, Tikhonchuk V T and Morreeuw J P 2004 Magnetic field generation in plasmas due to anisotropic laser heating *Phys. Plasmas* **11** 3830–9
- [12] Morreeuw J P, Sangam A, Dubroca B, Charrier P and Tikhonchuk V T 2006 Electron temperature anisotropy modeling and its effect on anisotropy–magnetic field coupling in an underdense laser heated plasma *J. Physique IV* **133** 295–300
- [13] Mochizuki T, Yabe T, Mima K, Yoshikawa K, Azechi H, Kikuchi A and Yamanaka C 1980 Ablation nonuniformity on laser irradiated pellet and collisional hot-electron filamentation *Japan. J. Appl. Phys.* **19** L645–8
- [14] Braginskii S I 1966 Transport processes in a plasma *Rev. Plasma Phys.* **1** 205
- [15] Borghesi M, Mackinnon A J, Bell A R, Gaillard R and Willi O 1998 Megagauss magnetic field generation and plasma jet formation on solid targets irradiated by an ultraintense picosecond laser pulse *Phys. Rev. Lett.* **81** 112–5
- [16] Froula D H *et al* 2007 Quenching of the nonlocal electron heat transport by large external magnetic fields in a laser-produced plasma measured with imaging thomson scattering *Phys. Rev. Lett.* **98** 135001
- [17] Nilson P M *et al* 2006 Magnetic reconnection and plasma dynamics in two-beam laser–solid interactions *Phys. Rev. Lett.* **97** 255001
- [18] Glenzer S H *et al* 1999 Thomson scattering from laser plasmas *Proc. 40th Annual Meeting of the Division of Plasma Physics of the American Physical Society (New Orleans, LA)* vol 6 (New York: AIP) pp 2117–28
- [19] Thomson J J 1978 Stimulated raman scatter in laser fusion target chambers *Phys. Fluids* **21** 2082–5
- [20] Kato Y, Mima K, Miyanaga N, Arinaga S, Kitagawa Y, Nakatsuka M and Yamanaka C 1984 Random phasing of high-power lasers for uniform target acceleration and plasma-instability suppression *Phys. Rev. Lett.* **53** 1057–60
- [21] Voronich I N 2001 Spatiotemporal smoothing of a laser beam employing a dynamic plasma phase plate *Quantum Electron.* **31** 970–2
- [22] Feugeas J-L, Nicolai Ph, Rieyre X, Schurtz G, Tikhonchuk V and Grech M 2008 Modeling of two-dimensional effects in hot spot relaxation in laser-produced plasmas *Phys. Plasmas* **15** 062701
- [23] Johnston T W 1960 Cartesian tensor scalar product and spherical harmonic expansions in Boltzmann's equation *Phys. Rev.* **120** 1103–11
- [24] Sangam A, Morreeuw J P and Tikhonchuk V T 2007 Anisotropic instability in a laser heated plasma *Phys. Plasmas* **14** 053111
- [25] Kingham R J and Bell A R 2004 An implicit Vlasov–Fokker–Planck code to model non-local electron transport in 2-d with magnetic fields *J. Comput. Phys.* **194** 1–34
- [26] Langdon A B 1980 Nonlinear inverse bremsstrahlung and heated-electron distributions *Phys. Rev. Lett.* **44** 575–9
- [27] Brantov A V, Bychenkov V Y, Tikhonchuk V T and Rozmus W 1998 Nonlocal electron transport in laser heated plasmas *Phys. Plasmas* **5** 2742–53
- [28] Ridgers C P, Kingham R J and Thomas A G R 2008 Magnetic cavitation and the reemergence of nonlocal transport in laser plasmas *Phys. Rev. Lett.* **100** 075003
- [29] Epperlein E M 1985 A comparison of the kinetic and 2-electron fluid models of the collisional Weibel instability in laser-plasmas *Plasma Phys. Control. Fusion* **27** 1027–35
- [30] Ridgers C P, Thomas A G R, Kingham R J and Robinson A P L 2008 Transport in the presence of inverse bremsstrahlung heating and magnetic fields *Phys. Plasmas* **15** 092311
- [31] Haines M G 1986 Magnetic-field generation in laser fusion and hot-electron transport *Can. J. Phys.* **64** 912–9
- [32] Matte J P and Virmont J 1982 Electron heat transport down steep temperature gradients *Phys. Rev. Lett.* **49** 1936–9